Elastic Flow Instability in Nanotube Suspensions

S. Lin-Gibson,[1] J. A. Pathak,[1] E. A. Grulke,[2] H. Wang,[1,3] and E. K. Hobbie[1,*]

[1]*National Institute of Standards and Technology, Gaithersburg, Maryland 20899, USA*

[2]*Department of Chemical Engineering, University of Kentucky, Lexington, Kentucky 40506, USA*

[3]*Department of Materials Science and Engineering, Michigan Technological University, Houghton, Michigan 49931, USA*

(Received 25 June 2003; published 29 January 2004)

We report an elastic instability associated with flow-induced clustering in semidilute non-Brownian colloidal nanotubes. Rheo-optical measurements are compared with simulations of mechanical flocculation in sheared fiber suspensions, and the evolving structure is characterized as a function of confinement and shear stress. The transient rheology is correlated with the evolution of highly elastic vorticity-aligned aggregates, with the underlying instability being somewhat ubiquitous in complex fluids.

DOI: 10.1103/PhysRevLett.92.048302 PACS numbers: 82.70.–y, 47.55.Kf, 61.46.+w

The clustering of small spherical particles has been studied extensively in a broad range of physical systems [1–6]. In contrast, little is known about the flocculation of asymmetrical particles, such as platelets, rods, or fibers. Given the current interest in dispersing anisotropic nanoparticles in organic materials, a deeper understanding seems warranted. An almost universal aspect of aggregation is interparticle attraction, but external hydrodynamic forces, often used to disperse such particles, can alone induce clustering in highly anisotropic suspensions. Non-Brownian repulsive fibers, for example, aggregate under shear via mechanical entanglement and friction [7]. In this Letter, we report an elastic instability associated with flow-induced clustering in semidilute non-Brownian colloidal nanotubes. Kinetic measurements under varied confinement and shear stress are compared with recent simulations of flocculation in flowing fiber suspensions [7], and we correlate the transient rheological response with the evolution of vorticity-aligned aggregates. Small-amplitude oscillatory shear reveals the internal elasticity of these clusters, with homogenized suspensions showing gel-like behavior at long time scales. The data suggest that the underlying instability is ubiquitous in a number of flowing complex fluids.

Multiwalled carbon nanotubes (MWNTs) were grown via chemical vapor deposition. An electron micrograph is shown in Fig. 1(a). Based on such measurements, the mean diameter is $d \approx 50$ nm (polydispersity ≈ 1.1). Because of their length and optical contrast, individual MWNTs are discernible in optical micrographs of 25× or higher, and from 200× images of thin-film dispersions, the mean length is $L \approx 12$ μm (polydispersity ≈ 2.0). The suspending polyisobutylene fluid (PIB, $M_n = 800$, $R_g \approx 1$ nm) is Newtonian, with a shear viscosity of 10 Pa-s at 25 °C. Dispersions are prepared by dissolving the PIB in sonicated MWNT-toluene suspensions, which are stirred continuously as the solvent is removed. Suspensions of primary interest contain 5×10^{-3} mass-fraction MWNT in PIB and are semidilute, with $nL^3 \approx (4/\pi)\phi_0(L/d)^2 \approx 125$ and $nL^2d \approx (4/\pi)\phi_0(L/d) \approx 0.5$, where n is the number of tubes per unit volume and $\phi_0 \approx 1.7 \times 10^{-3}$ is the volume fraction. The tubes in PIB are nonsedimenting.

Optical microscopy (5–25×) is used to observe the motion of MWNTs and the formation of aggregates under shear, with flow along the x axis, a constant velocity gradient along the y axis, and vorticity along the z axis. Measurements are taken in the x-z plane. The sample is confined between two parallel quartz plates separated by a variable gap, h, with a tolerance of ± 5 μm. The upper plate rotates at an angular speed that sets the shear rate, $\dot{\gamma} = \partial v_x/\partial y$, at a fixed point of observation. A

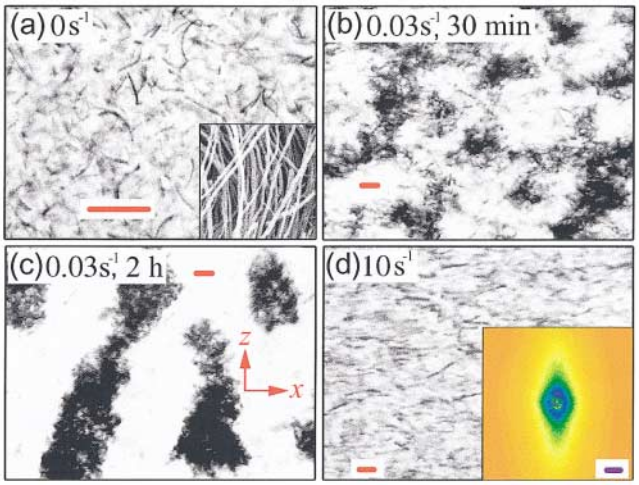

FIG. 1 (color). (a) Optical micrograph of a quiescent semidilute dispersion (0.5% MWNT by mass). The inset (width = 1.3 μm) is an SEM image before dispersion. Optical micrographs (b) 30 min after quenching the fluid to $\dot{\gamma}_0$, (c) 2 h after the quench, and (d) 15 min after quenching the sample in (c) to $\dot{\gamma}_m$. The aggregates have "melted" and the tubes orient with the flow, as evident in the depolarized light-scattering pattern (inset, scale bar = 1 μm^{-1}). The red scale bar is 10 μm and $h = 50$ μm.

controlled-strain rheometer [8] in cone-and-plate/parallel-plate configurations provides steady-shear measurements of the shear viscosity (η), shear stress (σ_{xy}, where σ_{ij} is the stress tensor), first normal stress difference ($N_1 = \sigma_{xx} - \sigma_{zz}$), and normal stress ($N = \sigma_{yy} - \sigma_{zz}$) under analogous flow conditions, as well as linear-viscoelastic measurements of the complex shear modulus, $G^*(\omega)$. All measurements were performed at 25 °C. The Reynolds number, $\mathrm{Re} \approx \dot{\gamma} h^2 \rho / \eta$ where ρ is the PIB mass density, is less than 10^{-3}.

Under weak shear, the tubes form macroscopic domains consisting of diffuse MWNT networks. Figure 1 shows optical micrographs of (a) a quiescent dispersion, (b),(c) aggregation at $\dot{\gamma}_0 = 0.03\ \mathrm{s}^{-1}$, and (d) redispersed MWNTs after subsequent dissolution at $\dot{\gamma}_m = 10\ \mathrm{s}^{-1}$, where light scattering [inset, Fig. 1(d)] reveals a steady-state distribution of orientations broadly peaked around $\hat{\mathbf{x}}$. For this value of h, $\dot{\gamma}_0$ lies just inside the region where confinement strongly influences domain coarsening, while $\dot{\gamma}_m$ is well inside the regime where the tubes do not aggregate. In simple shear, the long axis of an isolated rod rotates around $\hat{\mathbf{z}}$ with a period $\tau \propto \dot{\gamma}^{-1}$ [9,10]. In semidilute suspensions, hydrodynamic interactions determine the distribution of such orbits [11]. At $\dot{\gamma}_m$, particle-tracking measurements near the static lower plate yield $\tau_m \approx 8$ s, from which the period at $\dot{\gamma}_0$ is estimated to be $\tau_0 \approx 45$ min, an approximate time scale for clustering. The Peclet number at $\dot{\gamma}_0$ is [11] $\mathrm{Pe} \approx \pi \eta L^3 \dot{\gamma}_0 / \{3 k_B T (\ln r_p - 0.8)\} \approx 3 \times 10^4$, where $r_p = L/d$, implying that hydrodynamic forces overwhelm Brownian forces.

By varying h, we observe the transition from bulk to confined growth. To quantify the latter, we convert 5× micrographs into binary images in which the clusters are black and the surrounding fluid white (upper images, Fig. 2), defining a coarse composition field $\psi(\mathbf{r})$. Although the aggregates are diffuse, this provides a consistent measure of shape and position in the x-z plane. Ensembles at each annealing time, t, are used to compute the two-point correlation function, $c(\mathbf{r}) = \langle \psi(\mathbf{r}) \psi(0) \rangle$ (lower images, Fig. 2), and the steady-state morphology diagram in the h-$\dot{\gamma}$ plane is shown in the inset to Fig. 3(a). For "striped" patterns, multiple minima in $c(\mathbf{r})$ reflect periodicity along $\hat{\mathbf{x}}$. Figure 3 shows projections of $c(\mathbf{r})$ along $\hat{\mathbf{x}}$ and $\hat{\mathbf{z}}$ for the confined sample depicted in Figs. 1 and 2, with $c(x_i) \approx \exp(-2x_i/\xi_i)$ in the $x_i \to 0$ limit [12] giving the correlation lengths $\xi_x(t)$ and $\xi_z(t)$ [inset, Fig. 3(b)]. We find $\xi_z \propto t^{1/2}$, reminiscent of nonconserved

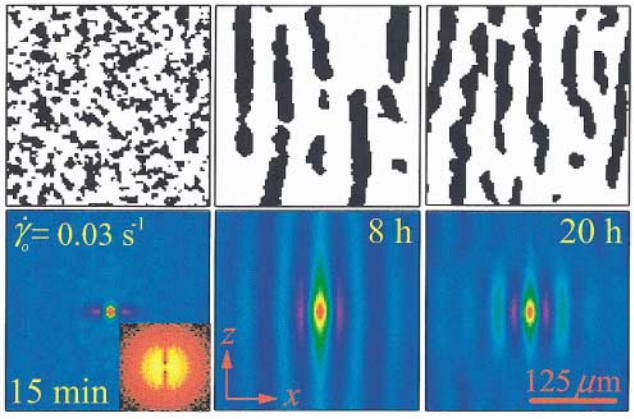

FIG. 2 (color). Evolution of a confined pattern for the sample depicted in Fig. 1 ($h = 50\ \mu$m). The lower images are the corresponding $c(\mathbf{r})$ at each t, where the red scale bar (125 μm) applies to all six images. The inset to the lower left image is its FFT (width = 1.2 $\mu\mathrm{m}^{-1}$), which gives the ubiquitous "butterfly" pattern.

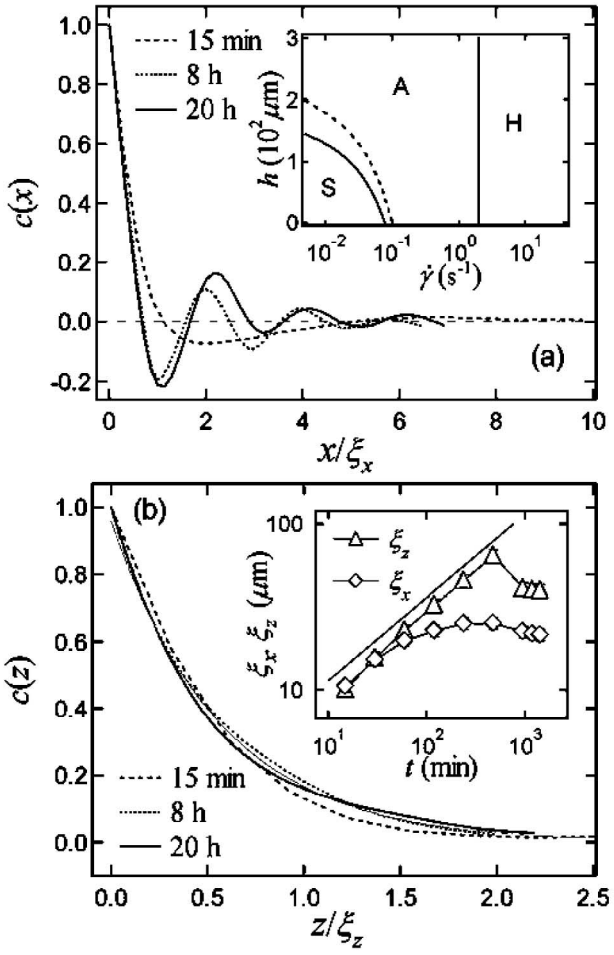

FIG. 3. Projections of $c(\mathbf{r})$ along (a) $\hat{\mathbf{x}}$ and (b) $\hat{\mathbf{z}}$ for the data in Fig. 2, where x and z have been reduced by the corresponding correlation length, shown in the inset to (b) with $t^{1/2}$. The gray curve in (b) is an exponential decay. The inset to (a) shows the measured "pattern diagram" (0.5% MWNT by mass) in the h-$\dot{\gamma}$ plane, with homogeneous (H), aggregated (A), and "striped" (S) regions. In region A, moderate aspect ratio domains are stable. In region S, these domains coarsen along $\hat{\mathbf{z}}$ into stripes. The dashed curve marks a region of "metastability" in which the stripes are transient. Roughly 50 measurements in the h-$\dot{\gamma}$ plane were used to deduce this diagram.

Ising-like growth [14], until both ξ_x and ξ_z start to *decrease* at late t. The mean area fraction of domains, $\alpha(t) = \langle \psi(\mathbf{r}) \rangle$, exhibits a maximum in the vicinity of $t/\tau_0 = 1.33$. Although $\xi_z \leq 60\ \mu$m and $\xi_x \leq 25\ \mu$m, domains larger than h are common at late t, and they tend to orient along $\hat{\mathbf{z}}$, rolling like logs in the x-y plane. Modeling these structures as monodisperse cylinders of diameter $\xi_y \approx \xi_x$, we approximate the volume fraction of domains via $\phi_d(t) \approx \pi\alpha(t)\xi_x(t)/4h$. The clusters are compressible and a late-t decrease in ϕ_d reflects an increase in density, with the internal MWNT mass-fraction growing from 3% (100 min) to 6% (24 h). This late-t contraction is also observed in region A.

The clustering has an intriguing rheological signature. Figure 4(a) shows η, N_1, and N (parallel plates, 100 μm gap) as a function of t after a quench to $\dot{\gamma}_0$, with 5× micrograph insets. The (upper) gray curve is $\eta(t) \approx \eta_0\{1 + [\eta]\phi_d(t) + \ldots\}$, where $[\eta] \approx 20$ is the intrinsic viscosity of domains and $\eta_0 \approx 10$ Pa-s is the viscosity of the homogenized suspension. The maximum in $\eta(t)$ and the transition to $N_1 < 0$ occur at $t \approx 60$ min ($t/\tau_0 = 1.33$), where $\phi_d(t)$ exhibits a maximum. Figure 4(b) is an analogous plot of subsequent "melting" at $\dot{\gamma}_m$, with a positive N_1 decaying to 5 Pa and η decaying to η_0, the former being consistent with modest steady-state tube deformation [15]. The domains quickly orient with the flow and dissolve. Although the measurements of N_1 in Fig. 4 are near the instrument resolution limit, the data are ensemble averages of multiple scans under identical flow conditions, and increasing the tube concentration (from 0.5% to 3% and 6% MWNT by mass) leads to negative N_1 values 10–100× larger in magnitude under analogous flow conditions. Negative first normal stress differences are uncommon. Associated with director tumbling in nematic liquid-crystalline polymers [11], their origin is not well understood [16–19]. Recently, $N_1 < 0$ has been linked to vorticity-aligned domains in attractive emulsions [20], suggesting an underlying similarity between these two markedly different systems.

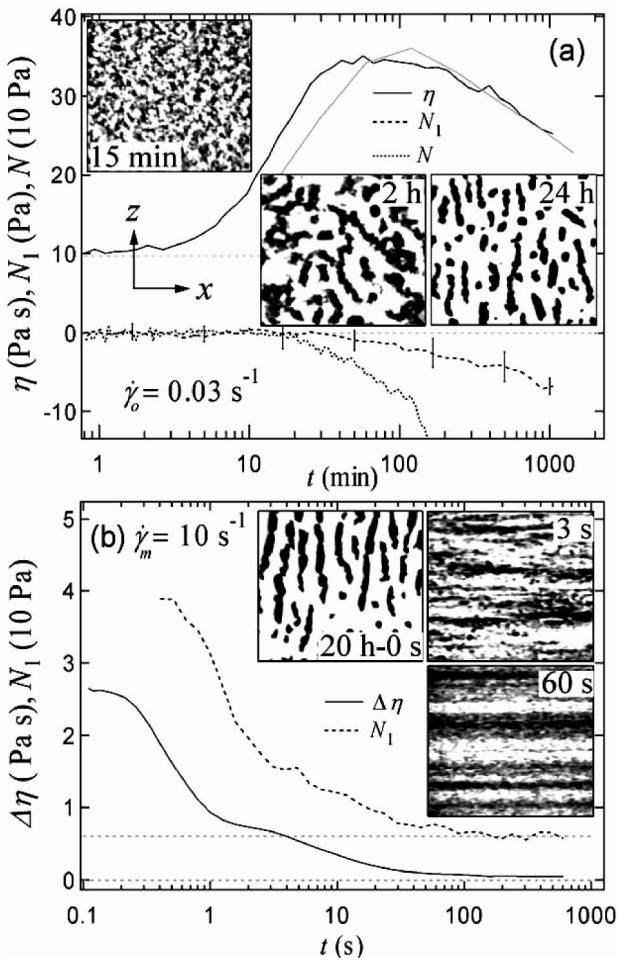

FIG. 4. (a) η, N_1, and N vs t at $\dot{\gamma}_0$. Inset images (width = 430 μm, $h = 50\ \mu$m) show the evolving morphology. (b) η and N_1 vs t following the quench of an aggregated sample (20 h at $\dot{\gamma}_0$) to $\dot{\gamma}_m$, where the clusters "melt." The viscosity of the rehomogenized suspension, η_0, has been subtracted from η. The upper gray curve in (a) is $\phi_d(t)$ scaled onto $\eta(t)$. Error bars show standard uncertainty.

Simulations of flow-induced flocculation in non-Brownian fiber suspensions suggest that friction leads to aggregation in the absence of attractive interactions, particularly at low shear stress and high stiffness, while an attractive potential leads to clusters that become less coherent as the stiffness increases [7]. The MWNT bending modulus can be compared with values for typical organic fibers [21], as can the interparticle potential and coefficient of friction [22]. Our measurements are in agreement with simulation. With an elastic bending modulus 10^3 times larger than that of a typical fiber, the MWNTs are flexible enough to deform in modest flows, yet they readily interlock to form coherent structures under weak shear. Held together by elastic forces, these diffuse clusters store sizable energy, which we infer from linear-viscoelastic measurements of the storage modulus, $G'(\omega)$, as a function of n [Fig. 5]. The solidlike response of homogeneous samples at 3% and 6% MWNT by mass reflects the network structure of the domains, and the interlocking of adjacent fibers might be a feature that distinguishes this type of flow-induced clustering from that observed, for example, during sedimentation [23,24].

We suggest that the response might be broadly viewed as a localized analog of "rod climbing" [25]. In this familiar instability, elastic forces acting along closed streamlines lead to an inward radial pressure that "squeezes" a viscoelastic fluid up a rotating shaft. The aggregates are soft elastic domains suspended in a less viscous fluid, and such an internal "hoop stress" in the x-y plane leads naturally to elongation along the z axis and, for compressible domains, contraction in the x-y plane (cartoon, Fig. 5). We note that the Weissenberg number, $\mathrm{Wi} = |N_1|/\sigma_{xy}$, is larger than 1 in the later stages of coarsening. Here, $N_1 < 0$ might arise from the

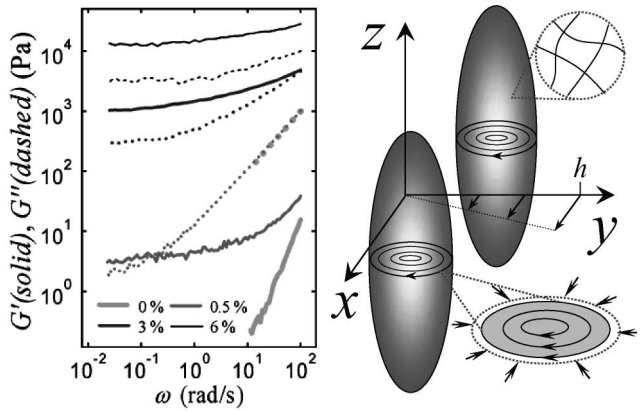

FIG. 5. The complex shear modulus, $G^*(\omega) = G'(\omega) + iG''(\omega)$, as a function of MWNT concentration for homogenized suspensions. The cartoon depicts the shear response of the compressible clusters, where internal streamlines are in tension due to elastic forces.

collective "pull" of contracting domains on the shearing surfaces. Limited by incompressibility and interfacial tension, a somewhat similar response is observed in sheared elastic emulsions [26]. Indeed, the early-t pattern (Fig. 2) appears in a host of flowing complex fluids, including polymer blends [13], semidilute polymer solutions [27], physical polymer gels [28], and thixotropic clay gels [29], all of which fall within the simple paradigm of interacting elastic domains suspended in a less viscous fluid. The homogenized dispersions also exhibit solidlike behavior at long time scales, reminiscent of other systems that exhibit this pattern [27–29]. The role of confinement in the growth of periodic structures is intriguing and merits computational consideration, which we hope this work will stimulate. A detailed study of the effect of varying tube concentration will be reported elsewhere.

We thank D. Klingenberg and M. Pasquali for useful discussions.

*Electronic address: erik.hobbie@nist.gov

[1] D. Fry, T. Sintes, A. Chakrabarti, and C. M. Sorensen, Phys. Rev. Lett. **89**, 148301 (2002).
[2] F. Leyvraz and S. Redner, Phys. Rev. Lett. **88**, 068301 (2002).
[3] S. Melle, M. A. Rubio, and G. Fuller, Phys. Rev. Lett. **87**, 115501 (2001).
[4] A. E. González, Phys. Rev. Lett. **86**, 1243 (2001).
[5] J. Blum *et al.*, Phys. Rev. Lett. **85**, 2426 (2000).
[6] E. K. Hobbie, Phys. Rev. Lett. **81**, 3996 (1998).
[7] C. F. Schmid and D. J. Klingenberg, Phys. Rev. Lett. **84**, 290 (2000); C. F. Schmid, L. H. Switzer, and D. J. Klingenberg, J. Rheol. **44**, 781 (2000).
[8] See C. R. Schultheisz, www.ts.nist.gov/ts/htdocs/230/232/232.htm SRM 2490 for instrument details.
[9] G. B. Jeffery, Proc. R. Soc. London, Ser. A **102**, 161 (1922).
[10] R. G. Cox, J. Fluid Mech. **45**, 625 (1971).
[11] R. G. Larson, *The Structure and Rheology of Complex Fluids* (Oxford University Press, New York, 1999).
[12] This anisotropic analog of the Debye model for two-phase random media [P. Debye, H. R. Anderson, and H. Brumberger, J. Appl. Phys. **28**, 679 (1957)] is derived in Ref. [13]. Although not random along $\hat{\mathbf{x}}$, interactions are less important for $x \to 0$.
[13] E. K. Hobbie *et al.*, J. Chem. Phys. **117**, 6350 (2002).
[14] A. J. Bray, Adv. Phys. **43**, 357 (1994). The binary field $\psi(\mathbf{r})$ has Ising symmetry and is not conserved.
[15] L. E. Becker and M. J. Shelley, Phys. Rev. Lett. **87**, 198301 (2001).
[16] G. Kiss, J. Polym. Sci. B **34**, 2263 (1996).
[17] C. E. Chaffey and R. S. Porter, J. Rheol. **29**, 281 (1985).
[18] G. Marrucci and P. L. Maffetone, Macromolecules **22**, 4076 (1989).
[19] R. G. Larson and M. Doi, J. Rheol. **35**, 379 (1991).
[20] A. Montesi, A. Pena, and M. Pasquali, Phys. Rev. Lett. (to be published).
[21] M. F. Yu *et al.* [Science **287**, 637 (2000)] measure the deformation of comparable MWNTs. The Young's modulus ($E_Y \approx 40$ GPa) and bending stiffness ($S = E_Y \pi d^4/2^6 \approx 1.22 \times 10^{-20}$ Nm^2) compare with 7.5 MPa and 8×10^{-12} Nm^2, respectively, for typical organic fibers [7]. The dimensionless bending stiffness, $S/(\eta_0 \dot{\gamma} L^4)$, and bending ratio, $E_Y\{\ln(2r_e) - 1.5\}d^4/(2\eta_0 \dot{\gamma} L^4)$, where $r_e = 1.24 r_p/\sqrt{\ln r_p}$, are 2 and 80, respectively, at $\dot{\gamma}_0$. At $\dot{\gamma}_m$, these are 0.006 and 0.24, respectively. For dimensionless bending ratios <1, the tubes deform [7,15].
[22] The toluene suspensions contain a succinimide polymer (1:1 MWNT by mass, PIB soluble) that acts as a dispersant via preferential wetting on the MWNT surface [C. Park *et al.*, Nanotechnology **14**, L11 (2003)]. These suspensions are only marginally stable, however, with weak flocculation occurring over the course of days, but gentle shaking redisperses the tubes, consistent with an attraction of order $k_B T$, and hydrodynamic forces dominate in the non-Brownian PIB suspensions of interest. The graphite-graphite coefficient of static friction (0.1) compares with 0.5 for typical organic fibers, but simulations suggest that attractive interactions lead to order-of-magnitude enhancement [7].
[23] B. Herzhaft *et al.*, Phys. Rev. Lett. **77**, 290 (1996).
[24] E. Kuusela, J. M. Lahtinen, and T. Ala-Nissila, Phys. Rev. Lett. **90**, 094502 (2003).
[25] F. H. Garner and A. H. Nissan, Nature (London) **158**, 634 (1946); K. Weissenberg, Nature (London) **159**, 310 (1947).
[26] E. K. Hobbie and K. B. Migler, Phys. Rev. Lett. **82**, 5393 (1999).
[27] E. Moses, T. Kume, and T. Hashimoto, Phys. Rev. Lett. **72**, 2037 (1994).
[28] S. Lin-Gibson *et al.*, J. Chem. Phys. **119**, 8080 (2003).
[29] F. Pignon, A. Magnin, and J.-M. Piau, Phys. Rev. Lett. **79**, 4689 (1997).